Korean J. Chem. Eng., 38(11), 2304-2312 (2021)
DOI: 10.1007/s11814-021-0891-4

pISSN: 0256-1115
eISSN: 1975-7220

Solubility measurement and preparation of nanoparticles of ampicillin using subcritical water precipitation method

Hadi Share Mohammadi, Ali Haghighi Asl†, and Maryam Khajenoori

Faculty of Chemical, Petroleum and Gas Engineering, Semnan University, Semnan 35131-19111, Iran
(*Received 11 February 2021 • Revised 23 June 2021 • Accepted 4 July 2021*)

Abstract−To improve the bioavailability of ampicillin trihydrate (AMP) as a poorly water-soluble drug, the nanonization of AMP particles was carried out by solvent anti-solvent precipitation for the first time. In this method the subcritical water (SW) and cold water at ambient conditions were utilized as the solvent and anti-solvent, respectively. At first, the solubility of AMP in SW was measured. The solubility of AMP in SW at a constant pressure of 5 MPa and the temperature range from 303.15 to 403.15 K was found to range from 0.380×10^{-3} to 17.689×10^{-3} mole fractions. The effects of three independent variables, including SW temperature, polyethylene glycol concentration, and anti-solvent temperature, on the particle size and morphology of the precipitated nanoparticles were studied. The obtained results of analyses confirmed that the AMP particles were nanosized to the smallest mean size of 66.5 nm using an environmentally friendly method without the requirement of organic solvents and related post-processing purification stages.

Keywords: Ampicillin Trihydrate, Subcritical Water, Solubility, Bioavailability, Nanoparticles

INTRODUCTION

Ampicillin trihydrate (AMP) is one of the vial antibiotics which is a derivative of the penicillin group. It is primarily prescribed to treat or prevent different types of diseases caused by bacteria, such as bronchitis, pneumonia, meningitis, sinusitis, and stomach, eye, bladder, lung, ear, skin, and urinary tract infections [1-3]. AMP inhibits the synthesis of the bacterial cell walls during active replication and leads to bactericidal activity against susceptible organisms [4]. It has been classified as a critically important antimicrobial and has exclusive properties, such as high activity, acid stability, and low toxicity [5]. However, AMP is poorly soluble in water (6 mg/ml at 293 K) [6]. Water solubility and dissolution rate are essential properties playing a vital role in the bioavailability of the drug [7]. The poor water solubility of AMP leads to low oral bioavailability after oral administration [8], which is an industry-wide problem for its development and optimal performance.

Many researches on poorly soluble drugs have confirmed that the dissolution rate, crystalline structure, and bioavailability of drugs can be enhanced by reducing particle size to the nanometer scale [9-12]. The nanonization of drug particles has some advantages: longer circulating capacity in the blood, elimination of unwanted side effects, and higher resistance against enzymatic degradation [13-16]. Accordingly, it is vital to produce AMP nanoparticles with a high dissolution rate and bioavailability for oral administration. Various methods have been proposed in the literature for particle size reduction to improve the dissolution rate, crystalline structure, and bioavailability of drugs; examples include high-pressure homogenization [17], milling [18,19], anti-solvent precipitation [20-23], and spraying process. The disadvantages of these conventional methods include high energy consumption, high solvent requirement, use of toxic organic solvents, and thermal degradation due to high shear forces [12].

During recent decades, supercritical fluid precipitation has also been utilized in several investigations to produce AMP micro and nanoparticles [24,25]. Tenorio et al. [2] generated AMP microparticles with the supercritical anti-solvent (SAS) technique. They used dimethyl sulfoxide, n-methyl pyrrolidone and ethyl alcohol as the solvent and supercritical carbon dioxide as the anti-solvent. The effect of solvent and experimental pressure on AMP particle size and particle size distribution was studied. The experimental results showed that a pressure change from 80 to 100 bar utilizing n-methylpyrrolidone, as the organic solvent, led to smaller mean particle size and better uniformity of particle shape. Nanoparticles of AMP have been precipitated by Montes et al. [26] via the SAS process. Spherical AMP nanoparticles were achieved with an average particle size in the range 218-360 nm. In their study, n-methyl pyrrolidone and supercritical carbon dioxide were utilized as the solvent and the anti-solvent, respectively. The concentration of liquid solution had the most significant influence on the particle size and particle size distribution. The authors reported that increasing the AMP initial concentration of the solution resulted in increased particle size with a broader distribution. Reverchon [3] proposed supercritical-assisted atomization (SAA) to prepare fine particles of AMP with a mean size of 0.1 to about 3.0 μm. In their work, methanol and supercritical carbon dioxide were implemented as the solvent and anti-solvent, respectively. The effect of SAA process parameters, including AMP concentrations in the liquid solvent, solvent flow ratios and nozzle diameters on particle shape, and particle size distribution of AMP microparticles, were investigated. Using water as the solvent led to larger AMP particles, whereas using methanol led to the preparation of smaller mean particle size of AMP

†To whom correspondence should be addressed.
E-mail: ahaghighi@semnan.ac.ir

with an average size of 0.4 μm. Esfandiari et al. [27] employed the supercritical gas anti-solvent (GAS) process to generate AMP microparticles. The effect of operating conditions, including solute concentration, pressure, temperature, and addition rate of anti-solvent, on particle size distribution, was examined. Solvent and anti-solvent were dimethyl sulfoxide (DMSO) and supercritical carbon dioxide, respectively. They obtained AMP nanoparticles with a mean particle size in the range of 220-430 nm. The pharmaceutical micronization of AMP using supercritical fluid techniques requires toxic solvents, which can be difficult to eliminate from the pharmaceutical compound matrix after size reduction and may cause environmental issues.

In the pharmaceutical industry, subcritical water (SW) technologies are new alternative supercritical fluid process and conventional precipitation methods that are promising for producing pharmaceutical nanoparticles. SW is usually known as liquid water heated to any temperature below its critical point at a sufficient pressure applied to maintain liquid phase [28,29]. The solubility of SW is strongly dependent on the temperature due to tunable water polarity. Water polarity has been observed to strongly rely on temperature [30]. The polarity of SW is reflected in the dielectric constant values [31]. As the water temperature is elevated above the boiling point, the water polarity reduces, therefore increasing its solvent power of non-polar organics and lower solvent power of polar organics [32]. An increase in temperature of water above 100 °C decreases the value of the dielectric constant. As a result, the water polarity becomes similar to conventional organic solvents, i.e., acetonitrile and dimethyl sulfoxide [33]. As a consequence of the ability to tune the value of water dielectric constant, it can be applied as a tunable solvent for hydrophobic organic compounds at different temperatures [34]. These exclusive properties of water can be utilized for producing ultrafine drug nanoparticles by solvent anti-solvent precipitation method [35]. Using SW as a green solvent overcomes many drawbacks linked to the use of organic solvents to dissolve hydrophobic organic compound for conventional solvent anti-solvent methods.

In general, the SW precipitation process is based on the difference in solubility of the drug in SW and water at room temperature. In this process, the hydrophobic compound is first dissolved in SW, and the solution is then sprayed into the water at room temperature using a nozzle with a 1 mm inner diameter. Thus, water is utilized both as a solvent of hydrophobic drugs (at subcritical conditions) and as an anti-solvent (at low temperature and pressure). By the rapid temperature quench of the solution, the polarity of the solvent is suddenly reduced. Since the solubility of hydrophobic drugs in SW can increase by up to ten orders of magnitude higher than that in water at room temperature, the rapid temperature variation causes a highly supersaturated zone when the temperature of SW-drug solution is rapidly decreased to room temperature. Consequently, the extremely high supersaturation allows to achieve homogeneous and rapid nucleation of the solute in the whole fluid and increase the nucleation rate, thus leading to fast precipitation of solute in the solvent medium [35]. In this study, polyethylene glycol (PEG) was chosen as a stabilizer. PEG is widely used as stabilizer in many types of pharmaceutical formulations for partially water-insoluble drugs. Accordingly, PEG was selected as stabilizer because of its non-toxic nature, ease of manufacture in the precipitation technique to achieve AMP nanoparticles with improved homogeneity of morphology and particle size distribution [36].

There is no experimental study on the production of AMP nanoparticles using SW processes. In the current work, for the first time, the feasibility of SW as the green process when applied to prepare AMP nanoparticles was examined. For this purpose, first, the solubility of AMP in SW using the static equilibrium method was examined experimentally. The solubility of AMP was determined at different temperatures from 303.15 to 403.15 K at a constant pressure of 5 MPa. Afterward, Box-Behnken design (BBD) was utilized to examine the effects of SW temperature, polyethylene glycol concentration, and anti-solvent temperature on AMP particle size. The processed and unprocessed AMP particles were investigated by X-ray diffraction (XRD), Fourier transform infrared spectroscopy (FTIR), scanning dynamic light scattering (DLS) and electron microscopy (SEM).

MATERIAL AND METHODS

1. Materials

Ampicillin trihydrate (purity >99.5%) was purchased from Antibiotic Sazi Iran Co. (Sari, Iran), and the required methanol with a purity of >99.9% was acquired from Merck (Germany). High-purity (99.99%) nitrogen was provided by Sabalan Co. (Tehran, Iran). Besides, the doubly distilled, deionized water purified using a Milli-Q deionizing unit (Millipore, USA) was utilized for all experiments.

2. Methods

2-1. Apparatus and Procedure of Solubility Measurement

A schematic of the experimental apparatus for static measurements of solubility of AMP is shown in Fig. 1. The laboratory setup included nitrogen cylinder, filters, equilibrium cell, magnetic stirrer, electrical band heater, collection vessel, water bath, temperature and pressure indicators, valves and control panel. Solubility measurement in this work was conducted in a solubility cell with an internal volume of 100 ml. Moreover, all components of equipment such as solubility cell, tubing and fitting, were made from stainless steel 316 to withstand high temperature and pressure of operating condition.

At the commencement of an experiment, the excess amount AMP and 50 ml water were introduced into the equilibrium cell together with a laboratory magnet. The amount of AMP loaded into the equilibrium cell was higher than the amount of solubilized during a solubility run (confirmed by inspecting the equilibrium cell after the solubility run for trace solute powder). To reduce solute degradation, water was degassed by bubbling a gentle stream of nitrogen. After this step, valve 1 and subsequently valve 2 were slightly opened, and nitrogen was released in the equilibrium cell. Valve 2 was closed when the nitrogen bubbles dripped out of the equipment. Observing the nitrogen overflow ensured that air was removed from the equipment. At the next stage, by opening valve 1, the system was pressurized with nitrogen at a pressure of 5 MPa. To maintain the solubility cell temperature at the designated values, an electrical band heater (OMEGA, DB-050772) was utilized and temperatures were regulated by a controller, which held the cell temperature within ±0.5 K. Once the set pressure and tempera-

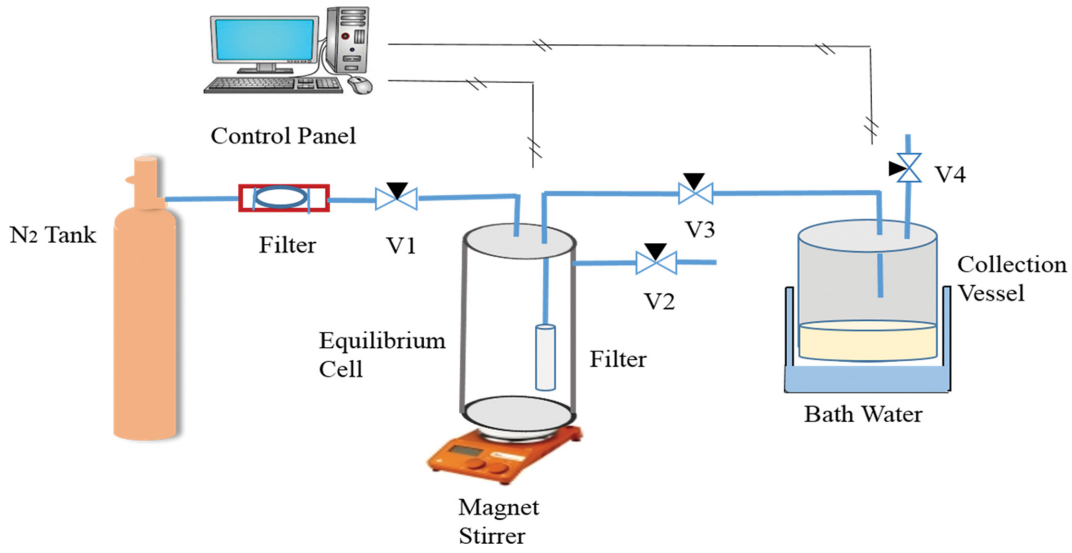

Fig. 1. Experimental apparatus for solubility measurement.

ture were reached, mixing was conducted utilizing the magnetic stirrer, and the contents of cells were mixed to achieve a better equilibrium condition and thereby accelerated mass transfer between solute and solvent. The static time was 5 min (as determined per elementary experiments) until there was no further enhancement in the value of the measured solubility at each solubility run and, consequently, solubility static time was verified.

At the end of the static time, the magnetic stirrer was turned off and valve 3 was fully opened to allow transfer of solution into the collection vessel with the nitrogen at 50 MPa acting to force the solution into the collection vessel. The solution was passed through a filter of 1 μm in pore size, which was placed in the equilibrium cell to retain the undissolved AMP inside the equilibrium cell. The presence of undissolved solute in the solubility cell was observed after each solubility run. The nitrogen at high pressure was applied to maintain the pressure of the equipment at a fixed value throughout the experiment. The use of nitrogen at the dominant pressure in the nitrogen tank (about 5 MPa) was used to maintain the solution in the liquid state and to avoid the premature evaporation of the solvent inside the equilibrium cell during the sampling.

When the solution was completely decanted from the equilibrium cell, valve 1 was shut, and the band heater was turned off. In the next stage, opening valve 4, the system was depressurized and the collection vessel was cooled with the water bath. The solvent and precipitated solute were collected from the collection vessel and were dried in the oven at 333 K. At the final stage, all of the paths located after the equilibrium cell were subjected to washing with 20 ml methanol to ensure all solutes were collected, and the solution was collected in a separate vial. The methanol solution obtained from washing was dried for 12 hours in the air.

Finally, the obtained solute from two vials dissolved at a certain value of methanol and analyzed by Halo-DB-20 UV-vis spectrophotometer (London, UK). AMP Solubility under different temperatures was determined by absorbance measurement at the wavelength range of 228 nm. Various standard solutions of AMP in methanol (5-25 μg/ml) were prepared. Subsequently, to calculate the solute concentration in the collection vials, a calibration curve with regression coefficients of 0.996 was developed. Three experimental measurements were conducted at each solubility data point to improve reliability. The measured solubility data is reported as the average values of three experimental runs with relative standard deviations smaller than 5%.

2-2. Box-Behnken Design

As a common response surface methodology (RSM) technique, the Box-Behnken experimental design (BBD) was implemented to evaluate the parameter affecting the production of AMP nanoparticles. BBD is an economical and useful design in industrial research because only three levels are needed for each factor [37]. This technique was employed to optimize the operating conditions for the production of AMP nanoparticles at the smallest possible size. The independent variables and their levels were selected according to initial tests. In this study, three independent variables, including SW temperature, PEG concentration, and anti-solvent temperature, were investigated at three levels. The statistical analysis of BBD was done via Design Expert software, version 7.0.0. To ensure reproducibility of the results, each precipitation run was performed in triplicates, and average values with relative standard deviations smaller than 5% were reported as particle size.

2-3. Apparatus and Procedure of SW Particle Formation

The experimental setup for the nanonization of AMP was developed from the apparatus utilized for the solubility measurement. An orifice nozzle with a 1 mm inner diameter was added to the collection vessel where precipitation occurred. For each experiment, 1 g of AMP and 50 ml water were inserted into the equilibrium cell. Opening valve 1, nitrogen at a constant pressure of 5 MPa was allowed to contact the equilibrium cell, and the system pressure was slowly increased with nitrogen at ambient temperature. After this, the system was heated to a required temperature utilizing an external electrical band heater. When the desired temperature and pressure were reached, cell contents were stirred using the magnet stirrer until equilibrium was achieved. After a static time (5 min), valve 3 was opened, and the solution was transferred into a nozzle situ-

ated inside the collection vessels. The line from the equilibrium cell to the precipitation vessel was 1/16 in. OD stainless steel tubing and designed at minimum length to minimize temperature drop before the collection vessel. Solution atomization was performed through the nozzle into a collection vessel (with 150 ml internal volume) equipped with water at low temperature or PEG solution (0.02, 0.04, and 0.06 wt%, respectively) as anti-solvent. The powders of AMP nanoparticles were separated from the suspension solution by centrifugation (12,000 rpm for 20 min) and dried in a vacuum oven at 323.15 K.

2-4. Characterization Techniques

In this study, AMP particles were characterized using scanning electron microscopy (SEM), Fourier transform infrared (FTIR) spectroscopy, dynamic light scattering (DLS), and X-Ray diffraction (XRD). FTIR spectra of samples were recorded from 500 to 4,000 cm^{-1} with an FTIR spectrometer (Thermo, AVATAR, USA) to establish the chemical stability of AMP. The standard KBr method was utilized [34]. The morphology of the AMP particles, including particle shape and surface characteristics, was determined by using the SEM analyzer (TESCAN, Mira III, Czech Republic). To prepare the AMP powder for the SEM image, the powder was sputter coated with gold palladium alloy. The particle size distribution of the AMP powder was determined by a DLS analyzer (Malvern, ZEN3600, UK). To prepare samples for the DLS analyzer, AMP was dispersed into deionized water. The powder XRD pattern of the processed and unprocessed AMP particles was measured by a X-ray diffractometer (Philips, PW1730, Netherlands) utilizing Cu radiation (λ=0.15405 nm) in the 2θ range of 10-80° with a step size of 0.05° and at 25 °C.

RESULTS AND DISCUSSION

1. Solubility of AMP in SW

In the present study, to reduce AMP degradation, water was degassed prior to solubility measurement. FTIR spectroscopy proved that no noticeable degradation of AMP in water solution was found at temperatures lower than 413.15 K. In other words, it was concluded that the chemical structure of AMP was stable under the experimental conditions used in this study. Accordingly, solubility measurement was conducted at a temperature below 403.15 K. In this study, the solubility of AMP in SW was determined within the temperature range of 303.15-403.15 K and the constant pressure of 5 MPa. The phase diagram of water is shown in Fig. 2. According to Fig. 2, water at a pressure of 5 MPa and temperature 303-403 K is in the liquid state. All solubility measurements and particle formation in the present study were conducted at a pressure of 5 MPa to keep a safe range away from the minimum pressure required to ensure water is in the liquid state.

Table 1 reports the measured solubility of AMP (equilibrium mole fraction, x_2) in SW as a function of the temperature (T). According to Fig. 3, the solubility of AMP in SW is enhanced exponentially with increasing temperature up to 403 K. After that, due to thermal degradation, the solubility of AMP decreases. The results (a dramatic enhancement in solubility with rising temperature) are consistent with the observations of other researchers for measuring the solubility of naproxen [38], ciprofloxacin [39], hydrophobic organic compounds [40], salicylic acids [41], and Parabens [42]. This resulted from a reduced dielectric constant of water and hence stronger solvating power of water for non-polar compounds at higher temperatures. When the temperature increased from 298.15 to 398.15 K, the dielectric constant of subcritical water significantly decreased from 78.6 to 49.5 [43]. The thermodynamic properties of water were governed primarily by chemical forces of attraction such as hydrogen bonding. The strength of hydrogen bonding is reflected

Table 1. Solubility of AMP in SW at various temperatures

T (K)	$x_2 \times 10^3$ (mole fraction)
303.15	0.380±0.011
323.15	0.635±0.012
373.15	1.082±0.030
383.15	5.151±0.120
393.15	12.873±0.323
403.15	17.689±0.310
413.15	17.268±0.312

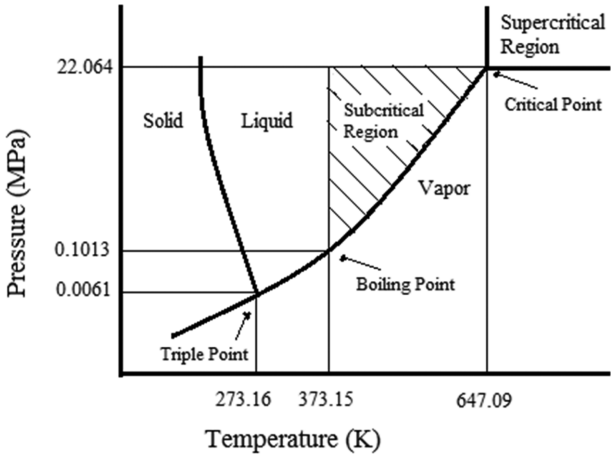

Fig. 2. Phase diagram of water as a function of temperature and pressure.

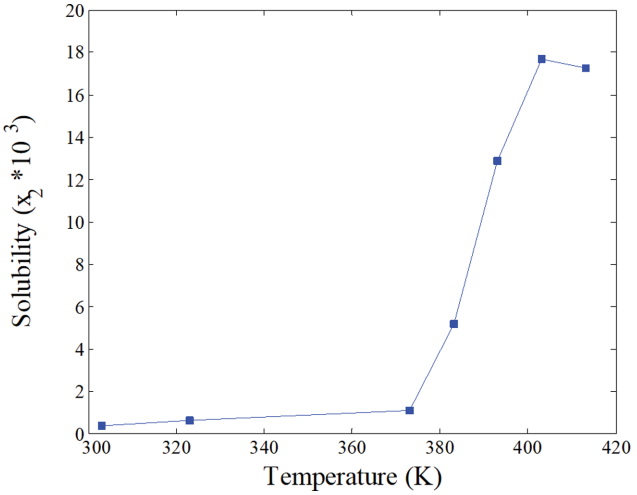

Fig. 3. Solubility of AMP in SW vs. temperature.

in the value of dielectric constant and heat of vaporization values. In general, hydrogen bonding is very dependent on temperature. Elevated temperature weakens the hydrogen bonds and decreases the dielectric constant value of water. In contrast, at low temperatures, the hydrogen bond strength is stronger and the dielectric constant value of water is higher, which tends to reduce the solvating power of water for hydrophobic compounds [44]. The reduction in the dielectric constant of water and hence water polarity, which consequently, contributes to the higher solubility of the hydrophobic compound in subcritical conditions. In this regard, Takebayashi et al. [45] proposed a two-parameter model relating solubility to the temperature at subcritical conditions and obtained good results in comparison to the literature. It is expressed as follows:

$$\mathrm{Ln}\,(x_2)=a+(bT) \quad (1)$$

where x_2 represents solute solubility in the mole fraction, T is the absolute temperature, a and b are the regressed parameters of the model.

However, the exponential solubility trend observed in Fig. 3 does not correspond with the rate of decline in the dielectric constant values of water, particularly the steep enhancement in solubility observed beyond 373 K. The change in solubility behavior may be related to termination in the hydrogen-bonds that form cages around solute molecules at 373 K, which hinders the solubility of materials in SW below 373 K [46]. The steep enhancement in solubility has been observed by other researchers [31,47,48]. Additionally, the result showed that at temperatures higher than 413 K, the solubility of AMP decreases, and it is likely that thermal degradation decreases the solubility of AMP.

2. Effect of Operating Parameters on Particle Size

In this study, three-level BBD from RSM was adopted to examine the effects of the SW temperature (373.15-393.15 K), PEG concentration (0.02-0.04 wt%), and anti-solvent temperature (273.15-303.15 K) on the morphology and mean size of the precipitated AMP particles. According to the BBD, the experimental results with an average of three replicates are listed in Table 2. Also, the pressure was fixed at 5 MPa. The mean particle size was determined by DLS.

The average particle size of the unprocessed AMP particles was about 30 μm and they had an irregular shape with a broad particle size distribution. The statistical analysis of BBD is presented in Table 3. The significance of each term was evaluated by the absolute probability values (p-values). A p-value of less than 0.05 indicates the model term has a significant effect on the process for a 95% confidence level. Moreover, if the F-value is higher than the model F-value, the statistical test is significant at a 95% confidence level. Based on the statistical analysis index, the most influential process variables affecting mean particle size are SW temperature, PEG concentration and anti-solvent temperature, respectively. Fur-

Table 2. Operation conditions of the SW processes and summary of the results

Run	SW temperature (K)	PEG concentration (PEG/water, wt%)	Anti-solvent temperature (K)	Mean size of particles (nm)
1	383.15	0.04	303.15	126.2
2	383.15	0.04	273.15	95.0
3	393.15	0.04	288.15	66.5
4	393.15	0.03	273.15	75.4
5	383.15	0.02	273.15	200.0
6	373.15	0.04	288.15	354.0
7	373.15	0.03	273.15	373.0
8	393.15	0.03	303.15	79.0
9	383.15	0.02	303.15	259.0
10	373.15	0.02	288.15	466.0
11	393.15	0.02	288.15	126.0
12	373.15	0.03	303.15	456.0

Table 3. BBD adequacy and ANOVA analysis

Source	Std. Dev.	R-square	Adjusted R-square	Predicted R-square	PRESS	Adequate precision
Model	17.40	0.9929	0.9870	0.9759	6,200.83	34.775
Source	Sum of squares	df	Mean Square	F -Value	P-Value	
Model	2.552×10^5	5	51,036.95	168.58	<0.0001	
C (PEG concentration)	20,940.81	1	20,940.81	69.17	0.0002	
Ts (SW temperature)	2.119×10^5	1	2.119×10^5	700.02	<0.0001	
Ta (anti-solvent temperature)	3,907.28	1	3,907.28	12.91	0.0115	
Ts.C	1,576.09	1	1,576.09	5.21	0.0627	
Ts^2	16,827.51	1	16,827.51	55.58	0.0003	

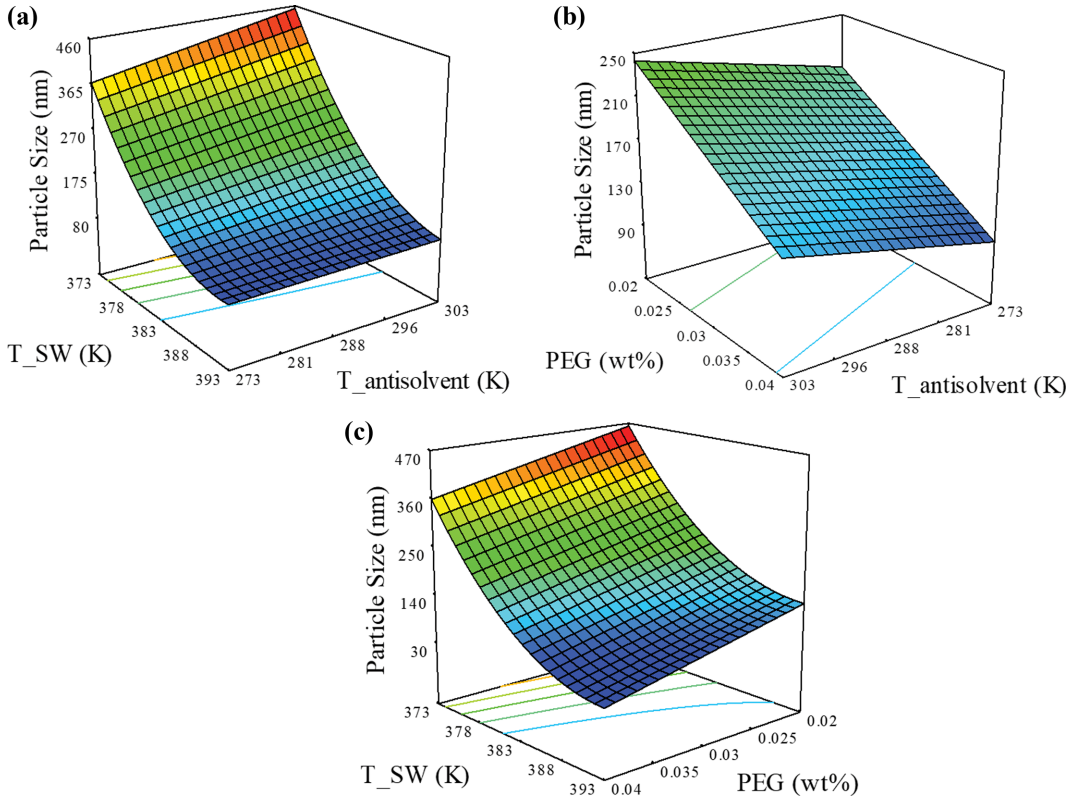

Fig. 4. AMP particle size as function of (a) SW temperature - anti-solvent temperature; (b) PEG concentration - anti-solvent temperature; (c) SW temperature - PEG concentration.

thermore, the calculated coefficient of determination R^2 (R-square), adjusted R^2, and predicted R^2 were 0.9929, 0.9870 and, 0.9759, respectively. The adequate precision shows the signal to noise ratio was obtained 34.775. A ratio greater than 4 is desirable and indicates an adequate signal. Consequently, taking all the statistical results into consideration, the model adequately represents the experimental data.

The influence of operating conditions, including SW temperature, PEG concentration, and anti-solvent temperature on the morphology and mean size of the precipitated AMP are shown in Figs. 4(a)-(c).

Continuing with the results, runs 3, 4, and 10 SEM images and corresponding DLS results are shown in Figs. 5(a)-(c).

2-1. Effect of SW Temperature

The effect of the SW temperature on the particle size of AMP was investigated by ranging it from 373.15 to 393.15 K, while pressure was held constant, with the results are shown in Figs. 4(a), (c). As can be seen, the mean particle size of AMP decreases as SW temperature increases. The temperature variation has a dual effect on the particle size. When the temperature was increased, the solid equilibrium solubility in subcritical water increased. In general, increased solubility may result in higher supersaturation of solute in subcritical media. According to nucleation theory, enhancement of solubility leads to high supersaturation of solute and low critical energy barrier, which leads to an increase in nucleation rate [49]. A rise in the nucleation rate might cause the formation of large amounts of crystals and lead to the formation of particles with smaller size [50,51]. On the other hand, with increasing temperature, the particle coagulation rate was drastically increased, and hence precipitated particle sizes may be enhanced. Due to these two competitive phenomena, no significant change was observed with increasing temperature up to 393 K. Several researchers have obtained similar results in terms of the effect of SW temperature on the particle size, confirming the results of the present work [50-54].

2-2. Effect of PEG Concentration

The effect of PEG concentration on the particle size of AMP is presented in Figs. 4(b), (c). Outputs demonstrate that an enhancement in PEG concentration from 0.02 to 0.04 wt%, decreased slightly the mean particle size of the precipitated AMP. This behavior can be explained by the fact that, during the formation of AMP nanoparticles, the PEG molecules effectively limited the aggregation and growth of AMP particles in the process of precipitation [51]. PEG molecules, because of the hydrophobic bond, adsorb on the surface of the AMP molecules and prevent the growth and aggregation of the AMP primary particles. By increasing the PEG concentration, more PEG molecules were adsorbed on the surface of AMP, and the interfacial tension of the AMP particles was reduced; consequently, the average particle size decreased. In our experiments, when the PEG concentration was raised to 0.03 wt%, the average particles size decreased slightly. This phenomenon can be explained that the AMP particles formed initially could no longer adsorb more PEG molecules. Similar results are presented by other researchers [34,52].

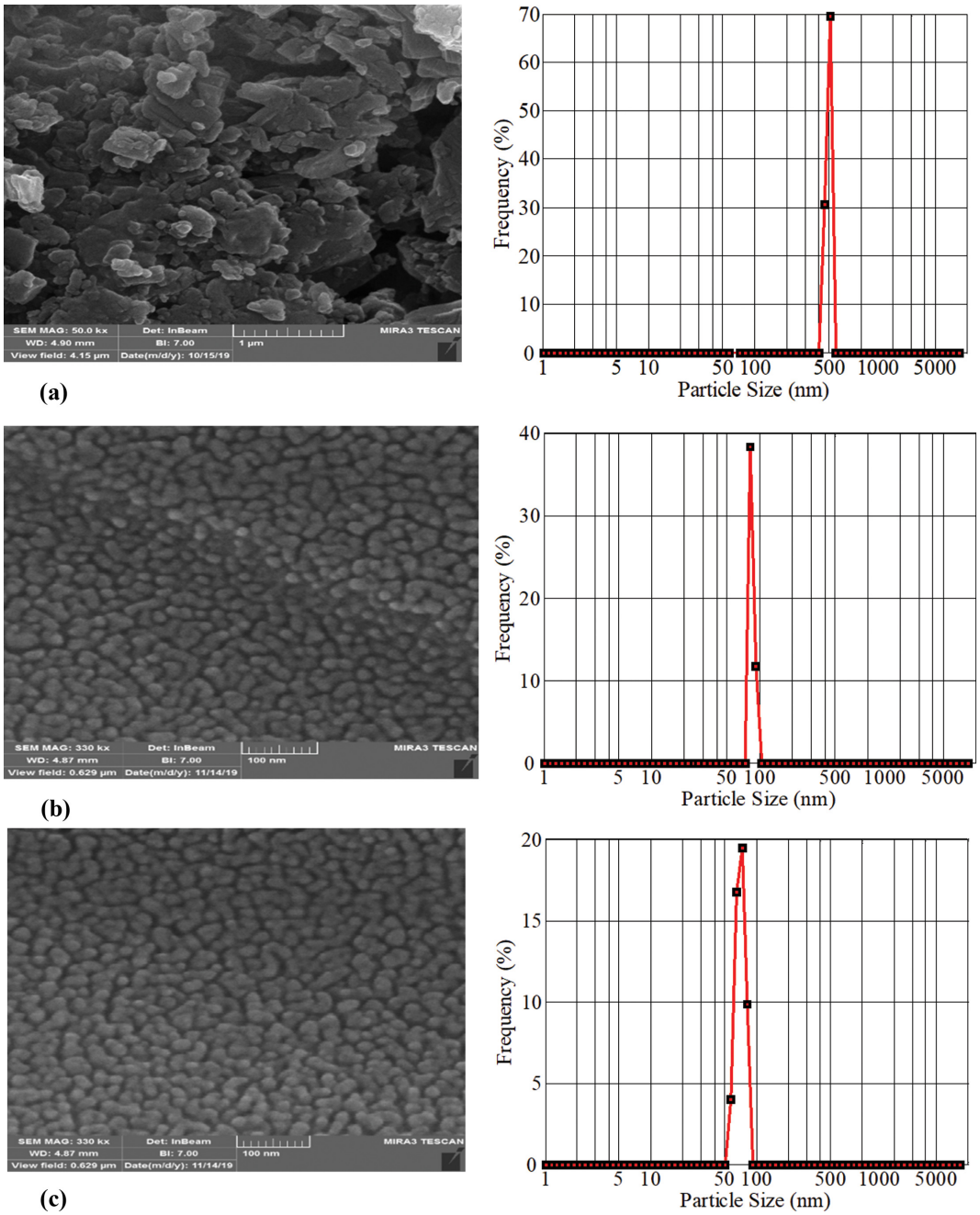

Fig. 5. SEM images and corresponding DLS particle size distributions for various conditions: (a) run 10; (b) run 4; (c) run 3.

2-3. Effect of Anti-solvent Temperature

Fig. 4(a), (b) depict the effects of anti-solvent temperature on the mean size of AMP particles. Clearly, with increasing anti-solvent temperature from 273.15 to 303.15 K, the average size of the precipitated AMP particles decreased. This observed trend could be explained as follows: by reducing the anti-solvent temperature, the solubility of the PEG in the water would fall, causing an enhancement in the level of supersaturation during the formation of AMP nanoparticles , therefore, with decreasing the anti-solvent temperature higher super-saturation was obtained, contributing to the formation of small particles. Additionally, the diffusion and the probability of particle collision decrease at low temperatures, led to the formation of smaller particles.

3. AMP Characterization

Fig. 6 demonstrates the XRD patterns of the processed and unprocessed AMP particles. Based on the results of XRD patterns, the processed AMP nanoparticles exhibited identical structure with lower peak area and intensity in comparison with that of the unprocessed AMP particles. Accordingly, the degree of crystallinity of the processed AMP particles was reduced after the nanonization process. The degree of crystallinity is an important factor for oral drugs. Compared to the crystalline state, a drug with low crystallinity is thermodynamically less stable. As a result, the dissolution rate of the drug increases. Results of the present study are in

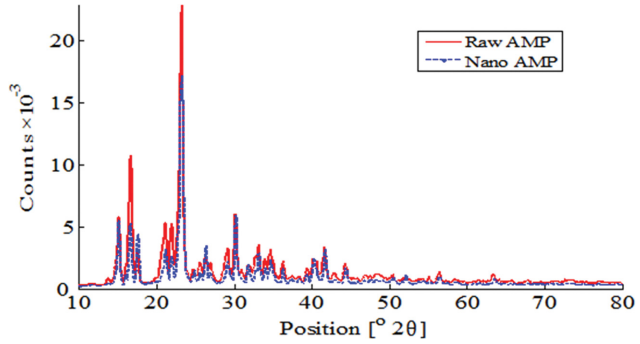

Fig. 6. XRD patterns for processed and unprocessed AMP particles.

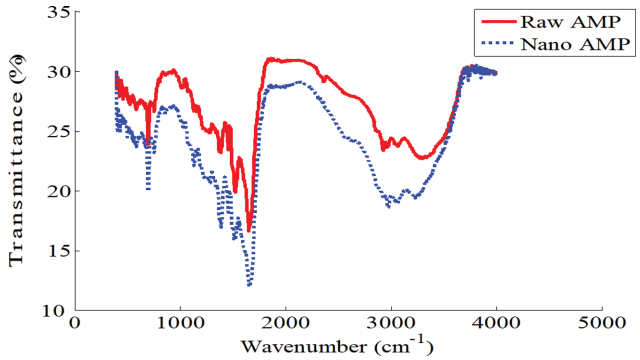

Fig. 7. FTIR spectra of processed and unprocessed AMP particles.

agreement with the results obtained by other researchers [10,11,51].

Fig. 7 presents the FTIR spectrum of the unprocessed and processed AMP particles. As shown, no significant difference in shape and position was observed between the absorption peaks obtained for the processed and unprocessed AMP particles. The results exhibit that the chemical composition of AMP did not affect the nanonization process and, also, the amount of PEG molecules that absorbed on the AMP particles surface was insignificant; the majority of the PEG molecules were eliminated during centrifugation of AMP suspension at the end of the process.

CONCLUSION

For the first time, solvent anti-solvent precipitation and SW were combined to prepare AMP nanoparticles. In this regard, the solubility of AMP was measured to mole fraction range from 0.380×10^{-3} to 17.689×10^{-3} in the temperature range of 303.15-403.15 K at a constant pressure of 5 MPa. Practically, AMP nanoparticles were successfully produced by the SW process in the range of 66.5-466.0 nm. Effects of the process parameters, including SW temperature (373.15-393.15 K), PEG concentration (0.02-0.04 wt%), and anti-solvent temperature (273.15-303.15 K), on the morphology and size of produced AMP particles were investigated with BBD. Based on statistical results from BBD, a decrease in anti-solvent temperature increases the particle size, whereas an enhancement in solvent temperature and PEG concentration decreases the particle size. In this study, the order of significance of investigated operating parameters affecting the particles size could be ranked as follows: SW temperature>PEG concentration>anti-solvent temperature. According to the results, the method applied in this study is a step forward in the size reduction of poorly water-soluble drugs, as it removes the requirement of organic solvents and linked post-processing purification stages. Future development of this technology should evaluate the costs involved in the scale-up of the process and compare them to conventional methods.

ABBREVIATIONS

AMP	: ampicillin trihydrate
SW	: subcritical water
SAS	: supercritical anti-solvent
SAA	: supercritical-assisted atomization
GAS	: supercritical gas anti-solvent
DMSO	: dimethyl sulfoxide
BBD	: Box-Behnken design
FTIR	: Fourier transform infrared spectroscopy
XRD	: X-ray diffraction
SEM	: scanning electron microscopy
DLS	: dynamic light scattering
PEG	: polyethylene glycol
x_2	: equilibrium mole fraction
T	: temperature [K]
RSM	: response surface methodology
R^2	: coefficient of determination

REFERENCES

1. G. Absalan, A. Abbaspour, M. Jafari, M. Nekoeinia and H. Ershadifar, *J. Iran. Chem. Soc.*, **12**, 879 (2015).
2. A. Tenorio, M. D. Gordillo, C. Pereyra and E. J. Martınez de la Ossa, *J. Supercrit. Fluids*, **40**, 308 (2007).
3. E. Reverchon, G. Della Porta and A. Spada, *J. Pharm. Pharmacol.*, **55**, 1465 (2003).
4. S. K. Sharma, L. Singh and S. Singh, *Sch. J. Appl. Med. Sci.*, **1**, 291 (2013).
5. Y. Fan, A. C. Pauer, A. A. Gonzales and H. Fenniri, *Int. J. Nanomedicine*, **14**, 7281 (2019).
6. J. W. Poole and C. K. Bahal, *J. Pharm. Sci.*, **57**, 1945 (1968).
7. Y. Wu, A. Loper, E. Landis, L. Hettrick, L. Novak, K. Lynn, C. Chen, K. Thompson, R. Higgins and U. Batra, *Int. J. Pharm.*, **285**, 135 (2004).
8. P. Khadka, J. Ro, H. Kim, I. Kim, J. T. Kim, H. Kim, J. M. Cho, G. Yun and J. Lee, *Asian J. Pharm. Sci.*, **9**, 304 (2014).
9. Y. Pu, J. X. Wang, D. Wang, N. R. Foster and J. F. Chen, *Chem. Eng. Process.*, **140**, 36 (2019).
10. G. Sodeifian, F. Razmimanesh and S. A. Sajadian, *J. Mol. Liq.*, **297**, 11740 (2020).
11. G. Sodeifian, S. A. Sajadian, N. S. Ardestani and F. Razmimanesh, *J. Supercrit. Fluids*, **147**, 241 (2019).
12. Z. Sayyar and H. Jafarizadeh-Malmiri, *Chem. Eng. Process*, **153**, 107938 (2020).
13. Q. Can, J. Carlfors and C. Turner, *Chin. J. Chem. Eng.*, **17**, 344 (2009).
14. O. Kayser, A. Lemke and N. Hernandez-Trejo, *Curr. Pharm. Biotechnol.*, **6**, 3 (2005).

15. C. Leuner and J. Dressman, *Eur. J. Pharm. Biopharm.*, **50**, 47 (2000).
16. S. Stolnik, L. Illum and S. Davis, *Adv. Drug Deliv. Rev.*, **16**, 195 (1995).
17. C. M. Keck and R. H. Muller, *Eur. J. Pharm. Biopharm.*, **62**, 3 (2006).
18. M. D. Louey, M. V. Oort and A. J. Hickey, *Pharm. Res.*, **21**, 1200 (2004).
19. N. Rasenack, H. Steckel and B. W. Muller, *J. Pharm. Sci.*, **92**, 35 (2003).
20. K. H. Song, C. H. Lee, J. S. Lim and Y. W. Lee, *Korean J. Chem. Eng.*, **19**, 139 (2002).
21. C. Chinnarasu, A. Montes, C. Pereyra, L. Casas, M. Teresa, C. Mantell, S. Pattabhi and E. Ossa, *Korean J. Chem. Eng.*, **33**, 594 (2016).
22. S. J. Park and S. D. Yeo, *Korean J. Chem. Eng.*, **25**, 575 (2008).
23. C. K. Kim, B. C. Lee, Y. W. Lee and H. Kim, *Korean J. Chem. Eng.*, **26**, 1125 (2009).
24. S. V. Dalvi and M. Mukhopadhyay, *Powder Technol.*, **195**, 190 (2009).
25. F. Masoodiyeh, J. Karimi-Sabet, A. R. Khanchi and M. R. Mozdianfard, *Powder Technol.*, **269**, 461 (2015).
26. A. Montes, A. I. Tenorio, M. D. Gordillo, C. M. Pereyra and E. J. Martinez, *Ind. Eng. Chem. Res.*, **50**, 2343 (2011).
27. N. Esfandiari and S. M. Ghoreishi, *AAPS Pharm. Sci. Tech.*, **6**, 1263 (2015).
28. M. Khajenoori, A. Haghighi Asl and F. Hormozi, *Chin. J. Chem. Eng.*, **17**, 359 (2009).
29. O. Ahmadi and H. Jafarizadeh-Malmiri, *Food Sci. Biotechnol.*, **29**, 783 (2020).
30. R. Alenezi, G. A. Leeke, R. C. D. Santos and A. R. Khan, *Chem. Eng. Res. Des.*, **87**, 867 (2009).
31. R. J. Fernandez-Prini, H. R. Corti and M. L. Japas, *High-temperature aqueous solutions: Thermodynamic properties*, CRC Press, Boca Raton (1992).
32. J. N. Park, A. Alinehari, H. C. Woo and B. S. Chun, *Korean J. Chem. Eng.*, **29**, 1604 (2012).
33. A. G. Carr, R. Mammucari and N. R. Foster, *Ind. Eng. Chem. Res.*, **49**, 3403 (2010).
34. H. Share Mohammadi, A. Haghighi Asl and M. Khajenoori, *Chin. J. Chem. Eng.*, **8**, 2620 (2020).
35. X. Y. Chen, Y. L. Shang, Y. H. Li, J. X. Wang, A. G. Maimouna, Y. X. Li, D. Zou, N. R. Foster, J. Yun and Y. Pu, *Chem. Eng. J.*, **263**, 20 (2015).
36. E. D. Hugger, B. L. Novak, P. S. Burton, K. L. Audus and R. T. Borchardt, *J. Pharm. Sci.*, **91**, 1991 (2002).
37. M. Rahimi, P. Valeh-e-Sheyda and H. Rashidi, *Korean J. Chem. Eng.*, **34**, 3017 (2017).
38. A. G. Carr, R. Mammucari and N. R. Foster, *Ind. Eng. Chem. Res.*, **49**, 9385 (2010).
39. Y. Pu, J. Lu, D. Wang, F. Cai, J. Wang, N. R. Foster and J. F. Chen, *Powder Technol.*, **321**, 197 (2017).
40. A. G. Carr, R. Mammucari and N. R. Foster, *Chem. Eng. J.*, **172**, 1 (2011).
41. B. Kayan, Y. Yang, E. J. Lindquist and A. M. Gizir, *J. Chem. Eng. Data*, **55**, 2229 (2010).
42. B. Kapalavavi, J. Ankney, M. Baucom and Y. Yang, *J. Chem. Eng. Data*, **59**, 912 (2014).
43. M. Uematsu and E. U. Frank, *J. Phys. Chem. Ref. Data*, **9**, 1291 (1980).
44. E. R. Caffarena and J. R. Grigera, *Physica A Stat. Mech. Appl.*, **342**, 34 (2004).
45. Y. Takebayashi, K. Sue, S. Yoda, Y. Hakuta and T. Furuya, *J. Chem. Eng. Data*, **57**, 1810 (2012).
46. K. Shinoda, *J. Phys. Chem. A*, **81**, 1300 (1977).
47. D. J. Miller and S. B. Hawthorne, *Anal. Chem.*, **70**, 1618 (1998).
48. S. Akay, B. Kayan, D. Cunbin, J. Wang and Y. Yang, *J. Mol. Liq.*, **253**, 270 (2018).
49. S. Karthika, T. Radhakrishnan and P. Kalaichelvi, *Cryst. Growth Des.*, **16**, 6663 (2016).
50. M. Turk, *J. Supercrit. Fluids*, **18**, 169 (2000).
51. G. Sodeifian, S. A. Sajadian and S. Daneshyan, *J. Supercrit. Fluids*, **140**, 72 (2018).
52. Y. Pu, Y. Li, D. Wang, N. R. Foster, J. X. Wang and J. F. Chen, *Powder Technol.*, **308**, 200 (2017).
53. Y. Pu, X. Wen, Y. Li, D. Wang, N. R. Foster and J. F. Chen, *Powder Technol.*, **305**, 125 (2017).
54. A. G. Carr, R. Mammucari and N. R. Foster, *Int. J. Pharm.*, **405**, 169 (2011).